processes

Article

Study on the Spatiotemporal Dynamic Evolution Law of a Deep Thick Hard Roof and Coal Seam

Zhigang Zhang [1,2], Linchao Dai [1,2,*], Haitao Sun [1,2,*], Yanbao Liu [1,2], Huiming Yang [1,2], Rifu Li [1,2] and Yi Zhang [1,2]

1 State Key Laboratory of the Gas Disaster Detecting, Preventing and Emergency Controlling, Chongqing 400037, China; zzg-2@163.com (Z.Z.); yanbao_liu@163.com (Y.L.); yhm3380@163.com (H.Y.); cqlirifu@163.com (R.L.); zy15896750887@126.com (Y.Z.)
2 China Coal Technology and Engineering Group, Chongqing Research Institute, Chongqing 400037, China
* Correspondence: 20212001047g@cqu.edu.cn (L.D.); dreamsht@163.com (H.S.); Tel.: +86-02365239611 (L.D.)

Abstract: Underground mining in coal mines causes strong disturbance to geological structures and releases a large amount of elastic strain energy. When the roof is a hard and thick rock layer, it is easy to cause dynamic disasters such as rock burst. To analyze the impact of a deep thick and hard roof fracture on the safe mining of thick coal seams, this paper studied the dynamic evolution process of the stress field, displacement field, energy field, and plastic zone of the coal seam and overlying strata during the mining process using FLAC3D numerical simulation. The results show that as the working face continues to be mined, the concentrated stress in the overlying strata first increases and then decreases, and the support pressure in front of the working face continues to increase. When it advances to 100 m, collapse occurs, and the stress increases sharply; the bottom plate undergoes plastic failure, resulting in floor heave. The overlying strata mass in the top plate exhibits downward vertical displacement, while the rock mass in the bottom plate exhibits upward vertical displacement, with a maximum subsidence of 4.51 m; energy concentration areas are generated around the working face roadway, forming an inverted "U" shape. When collapse occurs, the energy density decreases slightly; the direction of the plastic zone changes from "saddle shaped" to complete failure of the upper rock layer, and the overlying strata is mainly shear failure, which expands with the increase in mining distance. The research results have important practical significance for guiding the safe mining of deep thick and hard roof working faces.

Keywords: impact pressure; deep thick hard top plate; mining disturbances; numerical simulation

check for updates

Citation: Zhang, Z.; Dai, L.; Sun, H.; Liu, Y.; Yang, H.; Li, R.; Zhang, Y. Study on the Spatiotemporal Dynamic Evolution Law of a Deep Thick Hard Roof and Coal Seam. *Processes* **2023**, *11*, 3173. https://doi.org/10.3390/pr11113173

Academic Editors: Carlos Sierra Fernández, Feng Du, Aitao Zhou and Bo Li

Received: 18 October 2023
Revised: 2 November 2023
Accepted: 6 November 2023
Published: 7 November 2023

1. Introduction

China has abundant coal resources and a wide distribution area. Coal occupies a dominant position in the composition of disposable energy in China. With the rapid development of the social economy and the improvement in people's living standards, the demand for raw coal is also increasing year by year [1,2]. In recent years, with the gradual depletion in shallow mineral resources in mining areas in eastern China, deep mining has become an inevitable trend for future development. Due to various factors such as tectonic stress, self-weight of overlying load, and complex geological structure, there are significant differences in the stress field of the original rock in deep coal seams compared to shallow coal seams. The deep environment accumulates more elastic energy in the coal seam, roof, and floor, and their combined structures during coal seam disturbance, resulting in high energy in the deep and frequent occurrence of large-scale coal rock dynamic disasters [3–7]. Thick and hard roof slabs are distributed in more than half of China's mining areas, and the occurrence conditions of coal seams are relatively complex. Today, with the widespread use of fully mechanized mining technology, nearly 40% of fully mechanized mining faces have experienced the phenomenon of thick and hard roof falling violently for the first time [8–10].

Therefore, it is particularly important to master the temporal and spatial evolution law of overlying strata movement and energy under the condition of a deep thick and hard roof.

In recent years, many researchers at home and abroad have done a lot of work for the mining of coal seams under thick and hard roof conditions [11–13]. Ma et al. [14] used a variety of research methods to reveal the deformation and failure mechanism of roadway-surrounding rock in a gently inclined soft coal seam under different factors under the condition of a thick and hard roof, and put forward corresponding treatment plans. Wang et al. [15] studied the ground pressure behavior law of a fully mechanized top coal caving face under the condition of a shallow buried thick hard roof, and used fracturing technology to pre-crack the thick hard roof of the face, and achieved good results. Tan et al. [16] studied the mechanism of hard-roof-type rock burst, and the results showed that the two characteristics of stress mutation and energy increase can serve as important indicators of precursor information of rock burst. Zhang et al. [17] used a comprehensive research method to study the distribution law of mining-induced stress during the mining process of the working face. The results showed that the thick and hard roof overlying the coal seam is the main influencing factor of mining-induced stress, and the closer the coal seam is to the thick and hard roof, the more concentrated the mining-induced stress is. Kang et al. [18] used a comprehensive research method to study the failure and movement patterns of thick and hard roof structures, and obtained the deformation and stress distribution patterns of the roof. Liang et al. [19] established a mechanical analysis model to study the relationship between different influencing factors on the advanced fracture position and initial fracture distance of a thick and hard roof, and compared the analysis results with on-site monitoring data to verify the accuracy of the model. Li et al. [20] used five working faces of Chenghe No.2 Coal Mine as an example to study the failure mechanism of the roof and floor of the No.2 coal seam using a combination of on-site testing and numerical simulation. They also analyzed the distribution patterns of stress and displacement fields and plastic zone evolution characteristics of the roof and floor with different degrees of advancement of the working face. Xiong et al. [21] established a mechanical model for coal face failure under repeated mining conditions. Through similar simulation experiments and numerical simulation methods, the development of coal seam roof structure and surrounding rock fractures under repeated mining conditions was studied. The results showed that under the same roof pressure, the development of coal face fractures was more complete, the coal strength was lower, and the coal face was more prone to failure. Yang et al. [22] constructed a 3D physical simulation test under the condition of a thick and hard roof, and obtained the evolution law of the overburden displacement field and the dynamic evolution characteristics of "three belts" during thick seam mining. Bu et al. [23] constructed a mechanical model for the mining bearing capacity of a thick and hard roof, and from the perspective of energy, analyzed the relationship between the energy accumulated due to the fracture of the thick and hard roof in the mining area and the strong dynamic pressure manifestation, revealing the characteristics of the impact of the fracture instability of the thick and hard roof on the strong rock pressure manifestation.

In summary, when researching the instability of a coal seam under the conditions of a thick, hard roof, researchers both domestically and internationally primarily concentrate on one or two of the stress field, displacement field, and energy field, ignoring the investigation of the space–time evolution law of multiple fields. Numerical simulation techniques for engineering geology are maturing and getting better with the broad usage of computer technology. These techniques are also gradually being applied to solve engineering geological problems. The mutual verification between the results of numerical simulation calculations, experimental findings, and engineering practice has expanded the scope of problem solving in engineering geology, deepened the exploration of research topics, and effectively advanced the quantitative advancement of the engineering geological discipline [24–26]. Therefore, during the mining process of deep, thick, and hard roof working faces, this research employs FLAC3D V4.0 numerical simulation software to simulate and examine the dynamic evolution process of the stress field, displacement field, energy field, and plastic zone of the coal seam and overlaying strata. Additionally, the distribution law and process of mining stress and thick hard impact roof impact on the alteration of coal elastic energy under deep high-stress conditions were examined. Under the limit conditions of gas containing coal failure and instability (outburst), obtain the dynamic distribution state, dynamic transfer process, and superposition effect with the high-energy elastic performance of the thick and hard roof. Then, analyze the spatial dynamic evolution law of the stress field and energy field. The study's findings can serve as a guide for safe mining in comparable circumstances.

2. Three-Dimensional Numerical Model of Coal Seam in Deep Thick and Hard Roof Working Face

A growing number of researchers are turning to numerical simulation techniques to address engineering geology-related issues as the field's numerical simulation technology matures. Using three-dimensional rapid Lagrangian analysis technology, FLAC3D is a numerical modeling tool that accurately models the behavior of materials in yield, plastic flow, softening, and massive deformation. The program is extensively used because of its strong functionality and good universality. Its distinctive advantages have been shown, particularly in the research on major deformation, simulation of construction processes, and material elasticity and plasticity analyses. Because of this reason, this study analyzes the working face mining process using FLAC3D V4.0 software while a thick, hard ceiling is present.

2.1. Selection of Constitutive Model

The rock mass in this simulation is mainly composed of sandstone and mudstone, which exhibit obvious elastic–plastic deformation characteristics under different confining pressures. The failure modes of the rock include plastic failure, tensile failure, and shear failure. Therefore, a Mohr–Coulomb constitutive model can be used [27].

2.1.1. Mohr–Coulomb Incremental Elasticity Theory

The Mohr–Coulomb criterion in FLAC3D is represented by principal stress σ_1, σ_2, σ_3 and strain increment $\Delta\varepsilon_1$, $\Delta\varepsilon_2$, $\Delta\varepsilon_3$, respectively. The incremental expression of Hooke's law in terms of generalized stress and stress has the following form:

$$\begin{cases} \Delta\sigma_1 = \alpha_1\Delta\varepsilon_1^e + \alpha_2(\Delta\varepsilon_2^e + \Delta\varepsilon_3^e) \\ \Delta\sigma_2 = \alpha_1\Delta\varepsilon_2^e + \alpha_2(\Delta\varepsilon_1^e + \Delta\varepsilon_3^e) \\ \Delta\sigma_3 = \alpha_1\Delta\varepsilon_3^e + \alpha_2(\Delta\varepsilon_1^e + \Delta\varepsilon_2^e) \end{cases} \tag{1}$$

In the formula, $\Delta\varepsilon_i^e$ represents the increment of elastic strain; α_1 and α_2 are material constants defined in terms of the shear modulus, G, and bulk modulus, K, as follows:

$$\alpha_1 = K + (4/3)G \tag{2}$$

$$\alpha_2 = K - (2/3)G \tag{3}$$

2.1.2. Mohr–Coulomb Yield Criterion

The failure envelope defined by the Mohr–Coulomb yield function from point A to point B is

$$f^s = \sigma_1 - \sigma_3 N_\phi + 2c\sqrt{N_\phi} \tag{4}$$

The yield function of tensile stress from point B to point C is defined as

$$f^t = \sigma^t - \sigma_3 \tag{5}$$

In the formula, ϕ is the friction angle, c is the cohesion force, and σ^t is the tensile strength, and

$$N_\phi = \frac{1+\sin\phi}{1-\sin\phi} \tag{6}$$

As shown in Figure 1, when $f^s \geq 0$, the material will undergo shear failure. After reaching the yield limit, the material undergoes plastic deformation at a constant stress level [28]. In the state of tensile stress, if the tensile stress exceeds the tensile strength of the material, the material will fail. And the strength of the material cannot exceed the $\sigma^t_{\max}$ value defined below, namely

$$\sigma^t_{\max} = \frac{c}{\tan\phi} \tag{7}$$

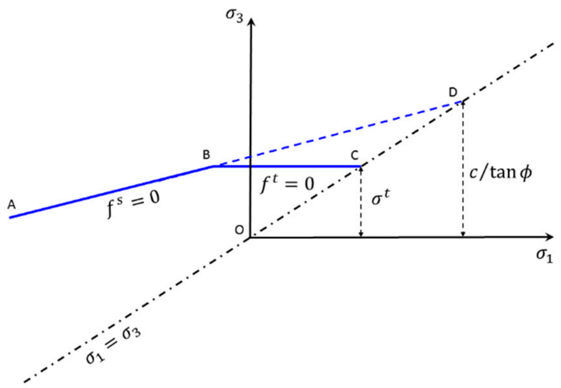

Figure 1. Mohr–Coulomb model of geotechnical materials and failure criteria.

2.1.3. Mohr–Coulomb Flow Criterion

The shear potential function g^s corresponds to the non-correlated flow law, namely

$$g^s = \sigma_1 - \sigma_3 N_\phi \tag{8}$$

The potential function g^t corresponds to the correlated flow law of tensile stress failure, namely

$$g^t = -\sigma_3 \tag{9}$$

For the case of shear tensile stress near the boundary, the flow criterion of the Mohr–Coulomb model can be used to calculate by defining a mixed yield function near the boundary in a three-dimensional stress space. Define function $h(\sigma_1, \sigma_3) = 0$ to represent the diagonal of the curves represented by $f^s = 0$ and $f^t = 0$ in the (σ_1, σ_3) plane. The expression for this function is

$$h = \sigma_3 - \sigma^t + \alpha^p(\sigma_1 - \sigma^p) \tag{10}$$

In the formula

$$\alpha^p = \sqrt{1 + N_\phi} + N_\phi \tag{11}$$

$$\sigma^p = \sigma^t N_\phi - 2c\sqrt{N_\phi} \tag{12}$$

The form of damage is represented by Zone 1 or Zone 2 in the (σ_1, σ_3) plane in Figure 2. If located in Zone 1, it is shear failure. Applying the flow criterion determined with potential function g^s, the stress points are regressed to the curve of $f^s = 0$. If located in Zone 2, it is tensile stress failure. Applying the flow criterion determined with potential function g^t, the stress points are regressed to the curve of $f^t = 0$ [29].

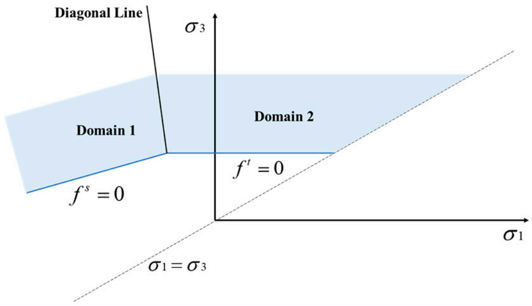

Figure 2. The area used in the Mohr–Coulomb model to define the flow criterion.

2.2. Establishment of a Three-Dimensional Numerical Model

The coal seam mined using a fully mechanized mining face in a certain coal mine had a gentle attitude and well-developed fractures. The thickness of the coal seam was 3.1~5.7 m, with a local thickness of 6.2 m and an average coal thickness of 4 m. The structure of the coal seam was relatively complex, containing 1~3 layers of gangue, and the lithology of the gangue was mostly siltstone. The dip angle of the coal seam was 0~10°, with an average of 4°. It was a nearly horizontal coal seam. The length of the working face was 150 m, and the burial depth of the working face was about 670 m. The roof of the coal seam was mainly composed of sandy mudstone and mudstone, while the floor was mainly composed of sandstone.

Taking the production geological conditions of the mining face as an example, a FLAC3D numerical physical model was established, as shown in Figure 3. The model size was 194 m × 150 m × 64 m, totally divided into five layers, of which the coal seam was 4 m thick. Because the coal seam was near horizontal, this simulation did not consider the issue of dip angle, and the dip angle of the coal seam was 0°. The number of zones generated was 159,840, and the number of grid points was 173,600. The *X*-axis direction of the model was defined as the inclination of the working face. The negative direction of the *Y*-axis was defined as the strike of the working face. The direction of rock deposits and reserves was defined as the *Z*-axis. A 10 m protective coal pillar was left in both the inclined and strike directions. This simulation used the Mohr–Coulomb constitutive model and activated the large deformation mode. Advance the mining along the *Y*-axis direction (mining direction of the working face), with a starting line of Y = 10 m and a mining step distance of 100 m. The mining was completed five times with a mining distance of 20 m. The boundaries around the model restricted horizontal displacement, with a fixed bottom and a free boundary at the top. A stress of 16 MPa was applied at the top to simulate the self-weight of the overlying strata. The lateral pressure coefficient was 1.1. The average unit weight of rock was 25 KN/m^3. The gas pressure was taken as 0.5 MPa [30,31]. The mechanical parameters used in the model are shown in Table 1.

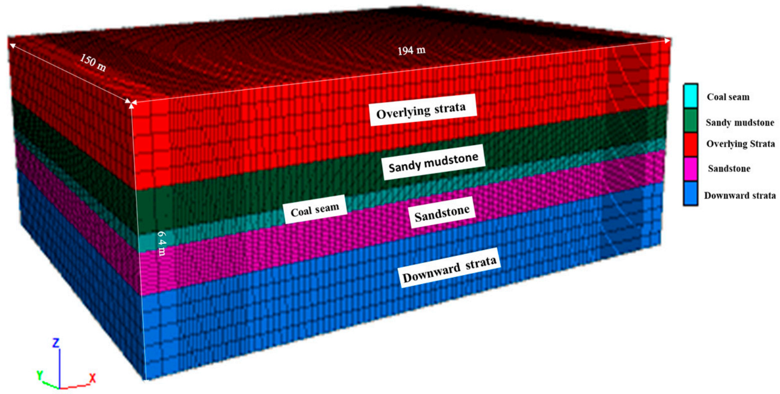

Figure 3. FLAC3D numerical physics model.

Table 1. Mechanical parameters of coal seam roof and floor.

Rock Strata	Thickness/(m)	Density/($kg \cdot m^{-3}$)	Friction Angle/(°)	Cohesion/MPa	Bulk Modulus/MPa	Shear Modulus/MPa	Tensile Strength/MPa
Overlying strata	20	1914	46.5	5.45	3.12	2.41	5.51
Sandy mudstone	10	2544.45	37.5	4.40	3.48	2.26	4.29
Coal seam	4	1625.75	24	3.30	1.52	0.81	1.25
Sandstone	10	2454	38.5	4.55	2.67	2.25	3.99
Downward strata	20	2314	46.5	5.45	2.41	2.41	5.41

3. Analysis of Numerical Simulation Results

This simulation studied the spatiotemporal evolution of the stress field, displacement field, energy field, and plastic zone in the coal seam and overlying strata of the deep thick and hard roof working face during the excavation process of the model Y = 10 m to Y = 110 m, with a mining distance of 100 m. In order to better display the spatiotemporal evolution laws of the stress field, displacement field, energy field, and plastic zone of the coal seam and overlying strata during the mining period of the deep thick and hard roof working face from multiple angles, a horizontal section is made for the overlying strata above the parallel coal seam, a vertical section is made for the parallel advancing direction, and monitoring lines are arranged at different distances from the bottom of the coal seam to monitor the changes in stress, displacement, and energy of the coal seam and overlying strata in real time every 20 m of advancing of the working face [32]. Three monitoring lines are arranged at Y = 115 m, with distances of 2 m, 12 m, and 22 m from the bottom of the coal seam, respectively; the total length of the monitoring line is 150 m, with a total of 16 monitoring points per layer, with a spacing of 10 m.

3.1. The Spatiotemporal Evolution Law of the Stress Field in the Coal Seam and Overlying Strata during the Mining Period of the Working Face

During the mining process of the working face, the stress field distribution of the overlying strata in the parallel and vertical directions of the working face is shown in Figures 4 and 5, respectively. The stress distribution of the overlying strata at different distances from the coal seam floor is shown in Figure 6.

As shown in Figures 4–6, as the working face continues to be mined, the support pressure in front of the working face continues to increase, leading to a gradual expansion of the scope of overlying strata failure; the farther away from the coal seam, the smaller the changes in overlying strata stress and displacement due to mining disturbance. As shown in Figure 4, as the working face advances, the stress concentration area of the overlying strata continues to expand, and the concentrated stress shows a trend of first increasing and then decreasing (it has increased from 25.7 MPa to 49.9 MPa and then decreased to 45.8 MPa). This is because collapse occurred when the excavation reached 100 m, resulting in partial stress release and a small decrease in concentrated stress. The overlying strata stress is mainly concentrated in the front of the working face and on both sides of the roadway. The stress in the overlying strata at the goaf is relatively low, which is the result of the movement of overlying strata during the extraction of coal seams. From Figure 4e, it can be seen that the mining of coal forms a goaf, and the stress in the surrounding coal and rock mass redistributes. The vertical stress around the mining face increases. As the roof collapses, the interior of the goaf is filled until it returns to the original rock stress state. From Figure 5, it can be seen that as the mining face continues to advance, the stress in the overlying strata behind the face gradually decreases, and the stress reduction area continues to expand. The overlying strata has a pressure relief zone, and the stress value gradually decreases with the coal seam mining and develops upwards. When the working face advances 100 m, collapse occurs and the stress increases sharply. As shown in Figure 6, when the advancing distance of the working face reaches 60 m, the stress in the overlying strata remains almost unchanged. When the advancing distance reaches 80 m, the stress increases slightly. When the advancing distance reaches 100 m, the stress at 2 m and 12 m away from the coal seam floor increases significantly, and the stress in the overlying strata at 22 m away from the coal seam floor changes sharply.

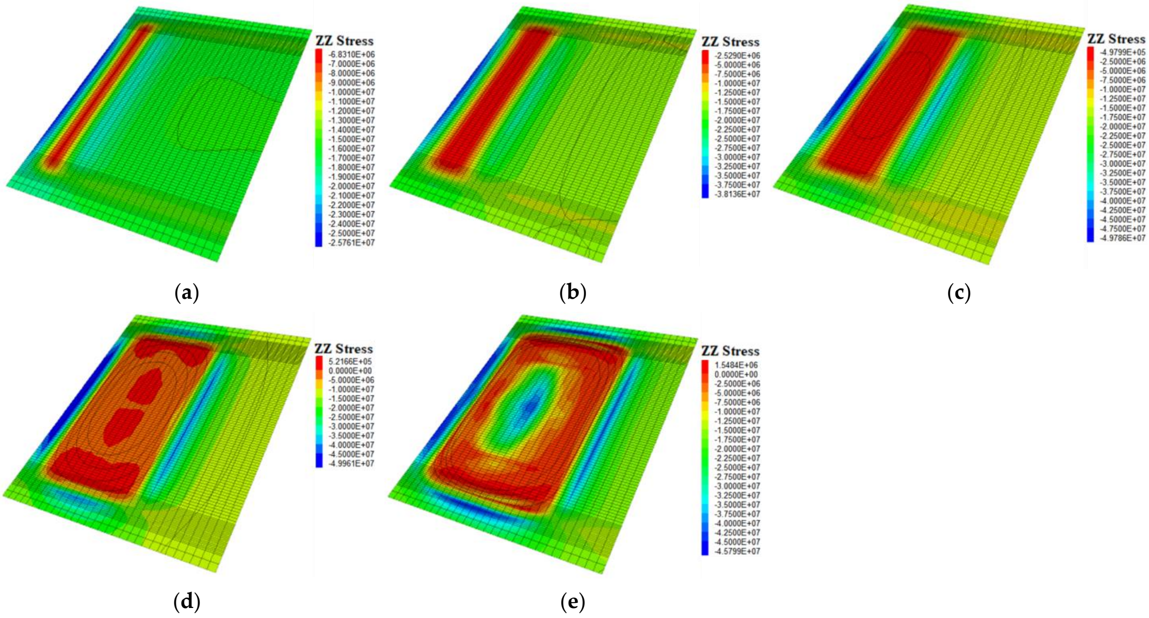

Figure 4. Spatial distribution of overburden stress at 12 m from the bottom of the coal seam during the remining period of the working face: (**a**) 20 m; (**b**) 40 m; (**c**) 60 m; (**d**) 80 m; (**e**) 100 m.

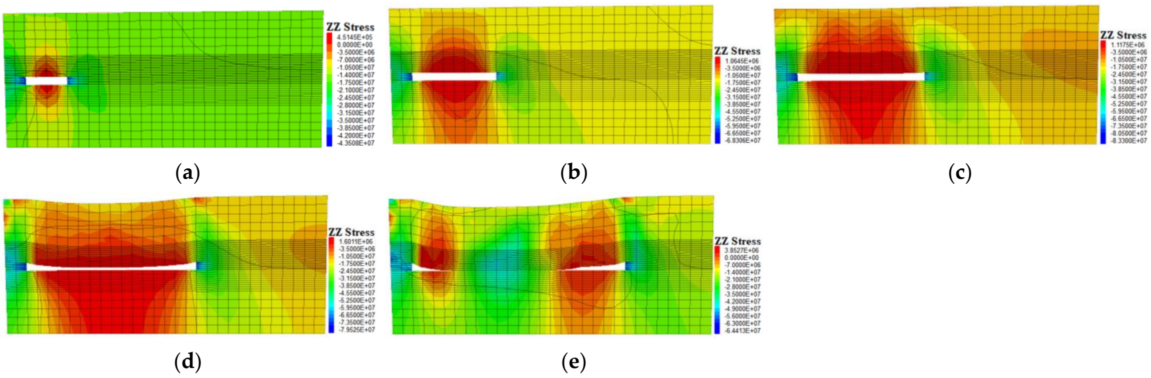

Figure 5. Overlying stress cloud along the direction of face advancement during face remining: (**a**) 20 m; (**b**) 40 m; (**c**) 60 m; (**d**) 80 m; (**e**) 100 m.

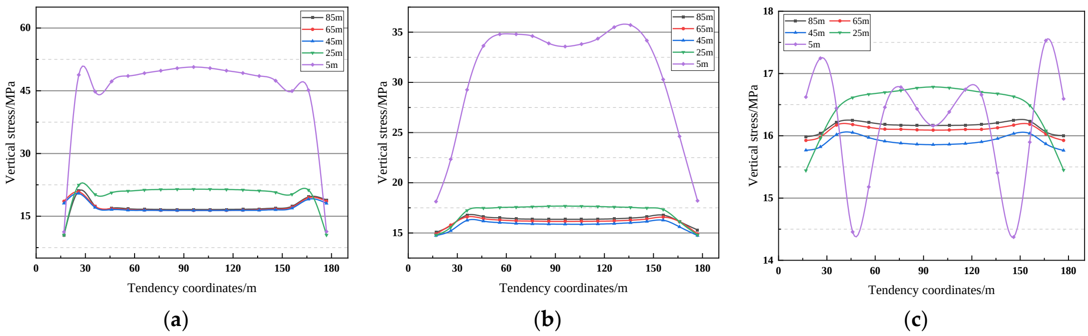

Figure 6. Vertical stress evolution results of overlying strata at different distances from the bottom of the coal seam during face remining: (**a**) 2 m; (**b**) 12 m; (**c**) 22 m.

3.2. The Spatiotemporal Evolution Law of the Displacement Field of Coal Seams and Overlying Strata during the Mining Period of the Working Face

During the mining process of the working face, the distribution of the displacement field of the overlying strata in the parallel and vertical directions of the working face is shown in Figures 7 and 8, and the distribution of the displacement curve of the overlying strata at different distances from the coal seam floor is shown in Figure 9.

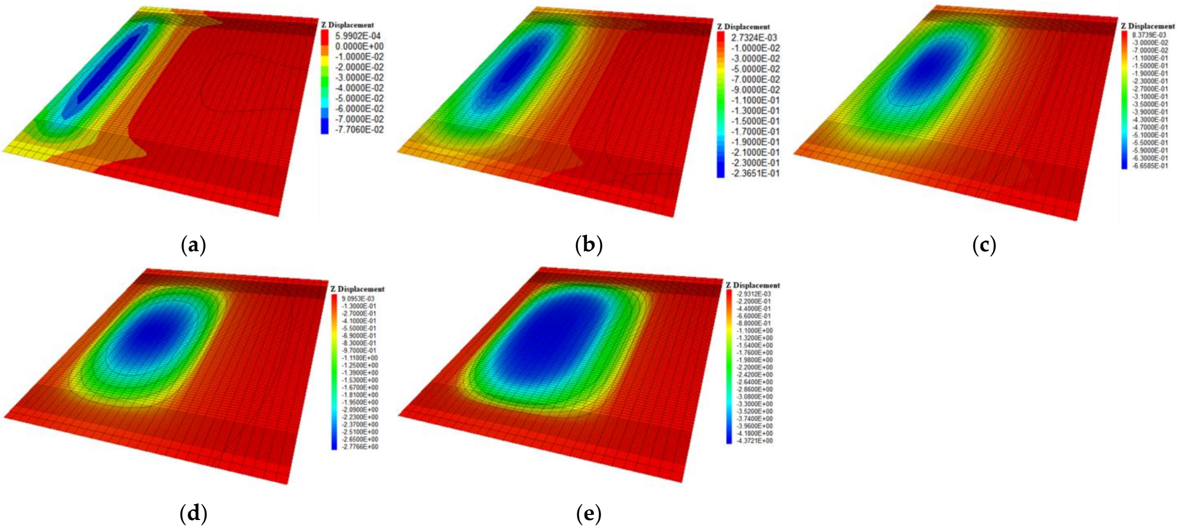

Figure 7. Spatial distribution of overburden movement at 12 m from the coal seam floor at different distances of the working face: (**a**) 20 m; (**b**) 40 m; (**c**) 60 m; (**d**) 80 m; (**e**) 100 m.

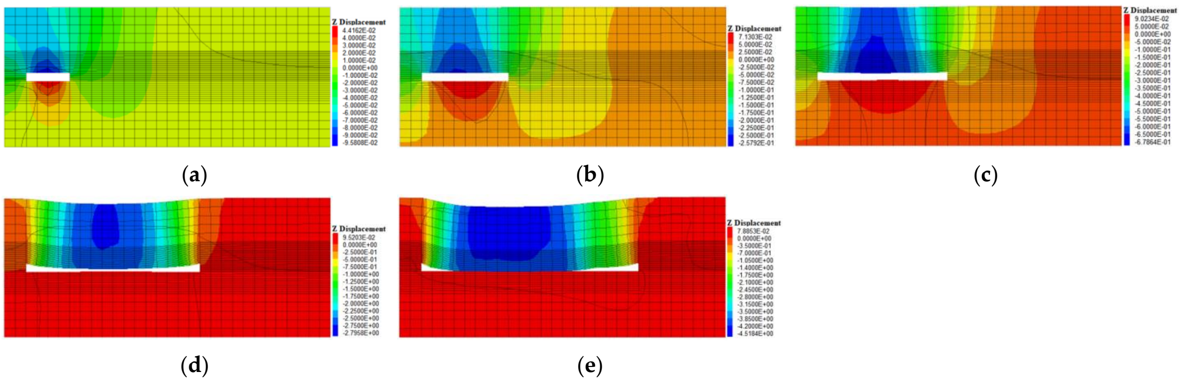

Figure 8. Overlying displacement cloud along the advance direction of the working face during the remining of the working face: (**a**) 20 m; (**b**) 40 m; (**c**) 60 m; (**d**) 80 m; (**e**) 100 m.

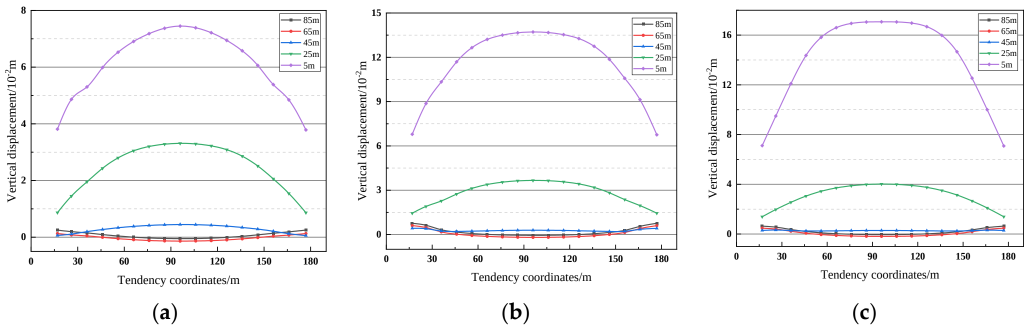

Figure 9. Evolution results of vertical displacement of overlying strata at different distances from the bottom of coal seam during the remining period of the working face: (**a**) 2 m; (**b**) 12 m; (**c**) 22 m.

From Figures 7 and 8, it can be seen that with the continuous mining of the working face, the rock mass on the top and bottom of the coal seam exhibits obvious displacement characteristics. The overlying strata mass in the working face roof mainly exhibits downward vertical displacement, while the rock mass in the bottom plate mainly exhibits upward vertical displacement. The displacement of the roof increases as the working face advances. When the working face advances to 80 m, there is a significant collapse, and when it advances to 100 m, there is a complete collapse with a maximum subsidence of 4.51 m. There was a significant upward displacement of the bottom plate at a distance of 80 m, increasing from 4.4 mm to the final 7.8 mm. This indicates that as the working face advances, the bottom plate undergoes plastic failure and produces a phenomenon of floor heave. From Figure 9, it can be seen that when the working face advances to 60 m, the displacement of the roof does not change significantly. When it advances to 80 m, the displacement slightly increases, while when it advances to 100 m, the displacement increases significantly. In addition, as the distance between the roof and the coal seam floor increases, its displacement also increases.

3.3. The Spatiotemporal Evolution Law of the Energy Field of Coal Seams and Overlying Strata during the Mining Period of the Working Face

During the mining process of this working face, the energy field distribution of the overlying strata in the parallel and vertical directions of the working face is shown in Figures 10 and 11, and the elastic energy distribution of the overlying strata at different distances from the coal seam floor is shown in Figure 12. The formula for calculating the elastic energy of the roof and coal seam is as follows:

$$U = \frac{\sigma_1^2 + \sigma_2^2 + \sigma_3^2 - 2\nu(\sigma_1\sigma_2 + \sigma_1\sigma_3 + \sigma_2\sigma_3)}{2E} \quad (13)$$

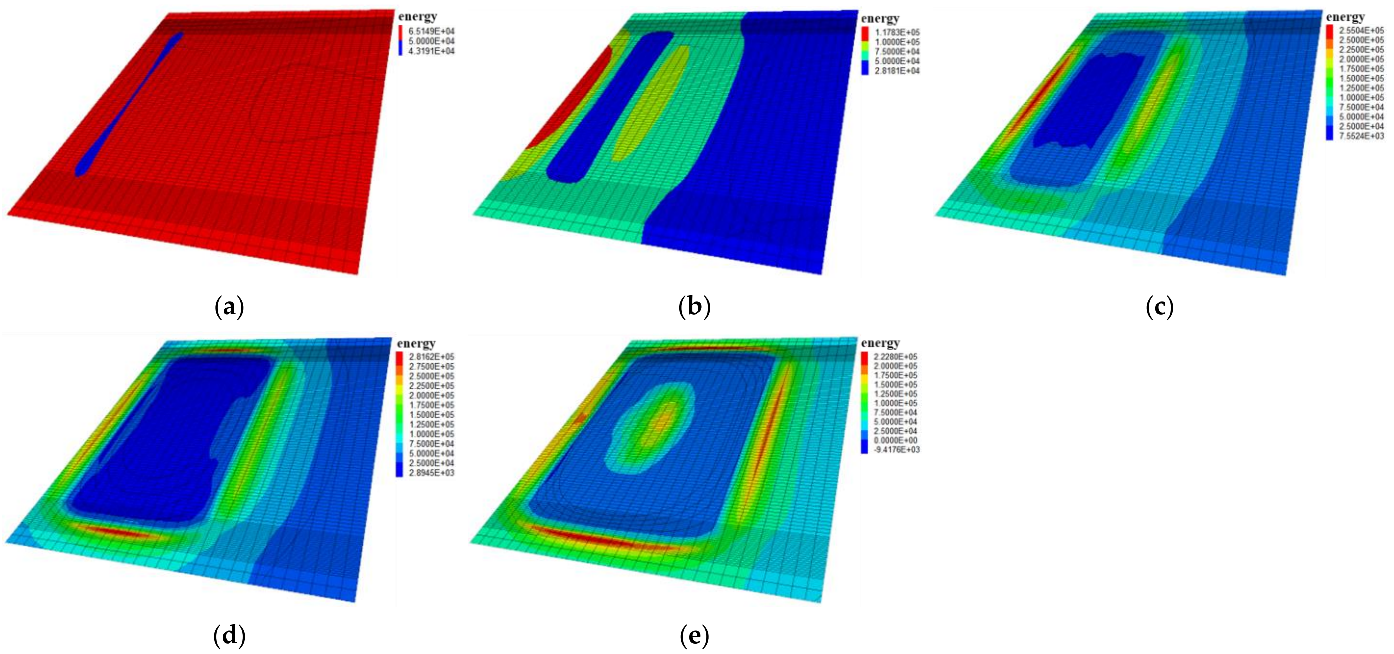

Figure 10. Energy distribution of overburden at 12 m from the bottom of the coal seam during the remining period of the working face: (**a**) 20 m; (**b**) 40 m; (**c**) 60 m; (**d**) 80 m; (**e**) 100 m.

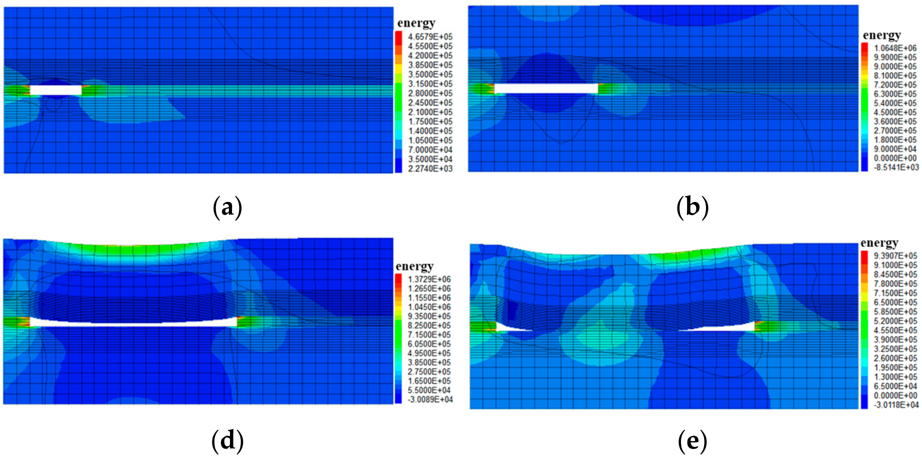

Figure 11. Cloud map of overlying elastic energy along the direction of face advancement during face remining: (**a**) 20 m; (**b**) 40 m; (**c**) 60 m; (**d**) 80 m; (**e**) 100 m.

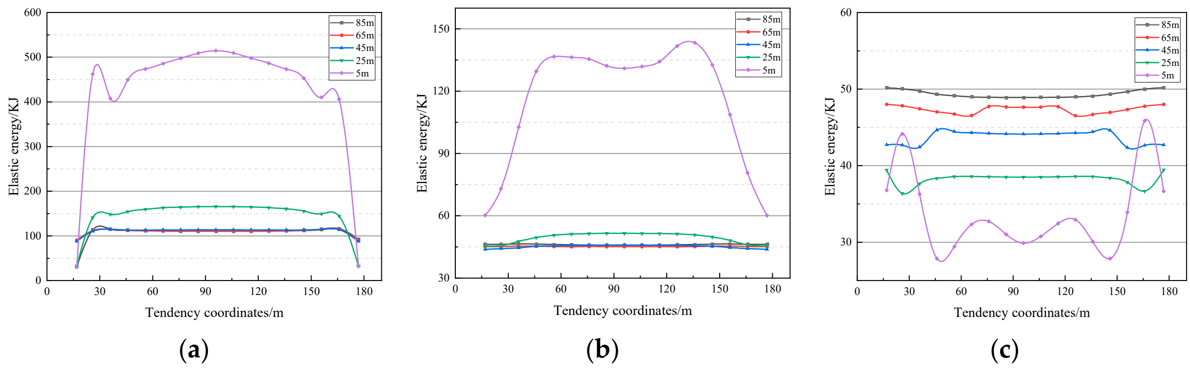

Figure 12. Evolution of elastic energy of overlying strata at different distances from the bottom of the coal seam during the recovery of the working face: (**a**) 2 m; (**b**) 12 m; (**c**) 22 m.

From Figures 10 and 11, it can be seen that the elastic energy after coal seam excavation is mainly concentrated in the overlying strata behind the working face and on both sides of the tunnel. Due to the soft nature of the coal body, the elastic deformation generated with the force is relatively large, and the stored elastic energy is relatively high, with a high energy density. Once the overlying strata is broken, the large amount of elastic energy stored in the coal and rock mass due to self-weight will be suddenly released, causing dangerous accidents. It can be seen that with the continuous mining of the working face, there is a significant energy concentration area around the working face roadway. When the working face is mined to 60 m, energy is connected at both ends of the roadway and the roof, forming an inverted "U" shape. And during the continuous mining process, this area also expands accordingly, reaching its maximum value when the working face advances to 100 m, but collapse occurs at this time and the energy density decreases slightly. From Figure 12, it can be seen that the upper and lower end areas are affected by the concentrated lateral support pressure of the mining face, resulting in energy accumulation. At a distance of 2 m and 12 m from the coal seam floor, a large amount of energy accumulation is generated in front of the working face due to mining disturbance, and the energy accumulation is relatively small at a distance of 22 m from the coal seam floor. Overall, the closer to the coal seam floor, the higher the accumulated elastic energy.

3.4. Plastic Failure Characteristics of Overlying Strata during Mining

From Figure 13, it can be seen that when the mining distance of the working face is short, the top and bottom rock layers undergo shear failure, a small portion undergoes tensile failure, and shear failure occurs in front of the coal wall and at the opening of the working face. As the working face continues to be mined, the height of plastic zone damage gradually increases, and the scope of damage gradually expands; when the working face is mined to a depth of 20 m, shear failure occurs in the top and bottom rock layers of the goaf. When mined to a depth of 40 m, a small amount of tensile failure occurs in the overlying strata of the roof. As the working face continues to advance, the scope of tensile failure gradually expands; as shown in Figure 13c, when the working face is mined to 60 m, the plastic zone of the overlying rock above the entire goaf presents a "saddle shaped" shape with high ends and a low middle, and the plastic zone is mainly characterized by shear failure. As shown in Figure 13d,e, with the mining of the working face, the plastic zone changes from "saddle shaped" to a direction where all the rock layers in the upper part of the goaf are destroyed. This is because when the mining reaches 80 m, the overlying strata above the goaf undergoes significant subsidence, the stress balance of the sur-rounding rock is disrupted, and the stress is redistributed, leading to further expansion of the height of the plastic zone on the roof until it penetrates.

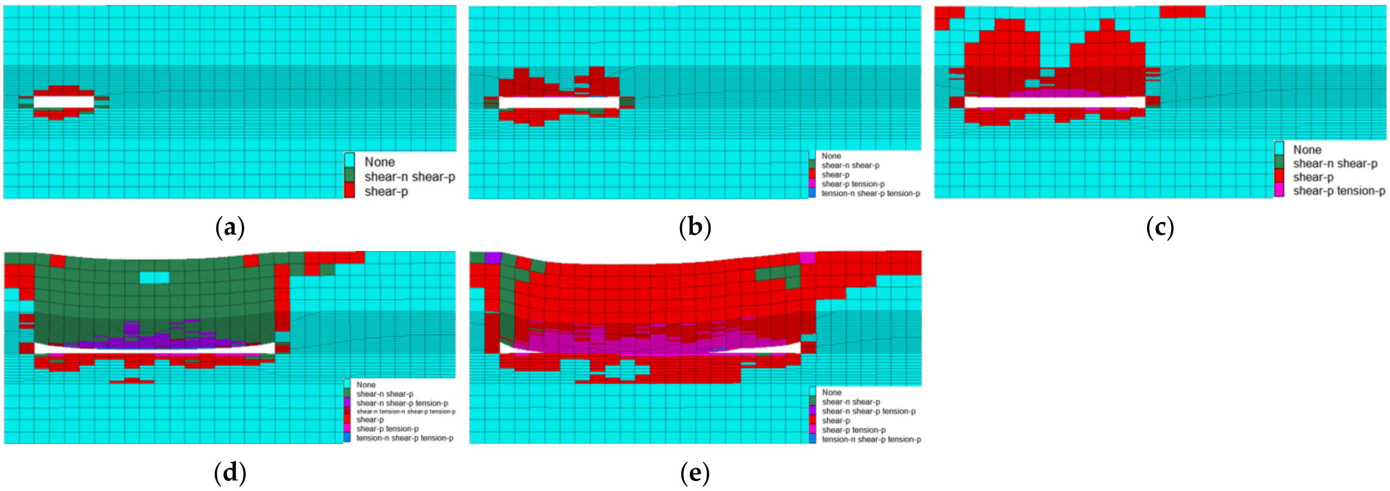

Figure 13. Development characteristics of overlying plastic zone above goaf during face remining: (**a**) 20 m; (**b**) 40 m; (**c**) 60 m; (**d**) 80 m; (**e**) 100 m.

3.5. The Distribution Characteristics of Stress, Displacement, and Plastic Zone in the Coal Seam and Overlying Strata in the Central Goaf

When the working face is mined to a depth of Y = 110 m, the vertical stress, displacement, and plastic zone distribution of the overlying rock in the middle of the goaf at Y = 60 m are shown in Figure 14.

From Figure 14a,b, it can be seen that in the middle of the working face, the overlying strata completely collapses and its vertical stress and displacement reach their maximum, decreasing towards both sides. From Figure 14c, it can be seen that the plastic zone exhibits a typical symmetrical distribution pattern with a larger range of roof failure and smaller two sides. The top plate undergoes tensile shear failure, the overlying strata undergoes large-scale shear failure, and the bottom plate undergoes small-scale shear failure.

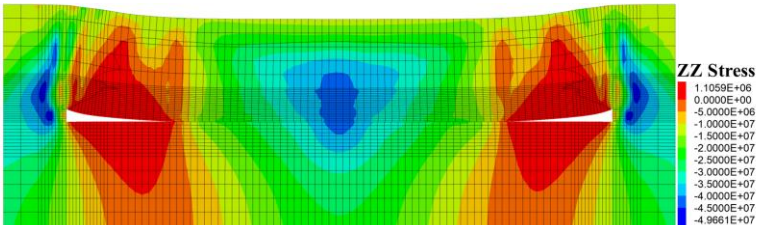

(**a**)

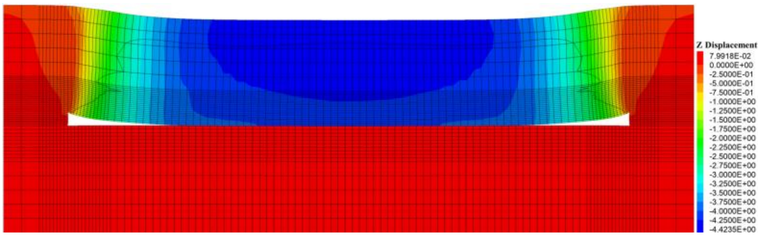

(**b**)

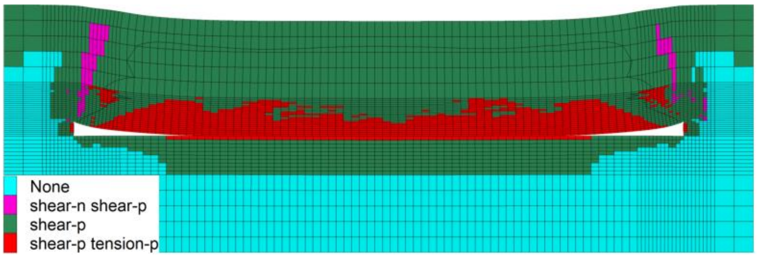

(**c**)

Figure 14. Distribution of stress, displacement, and plastic zone of the surrounding rock of the top and bottom slabs in the goaf area behind the working face: (**a**) Vertical stress diagram of overlying strata in goaf; (**b**) Displacement map of overlying strata in goaf; (**c**) Distribution of plastic zone of overlying strata in goaf.

4. Discussion

This study introduces the stress, displacement, and energy evolution characteristics of coal seam mining under the condition of a thick and hard roof. FLAC3D, as a simulation research tool, utilizes three-dimensional fast Lagrangian analysis technology and built-in multiple rock mechanics models. It can simulate the mechanical behavior of different types of rocks and soils, accurately simulating the behavior of materials in yield, plastic flow, softening, and large deformation. Moreover, it provides an intuitive graphical user interface that supports parallel computing, greatly improving work efficiency and demonstrating its unique advantages. Therefore, this article systematically analyzes the dynamic evolution process of the stress field, displacement field, energy field, and plastic zone of the coal seam and overlying rock during the mining process of the working face using FLAC3D V4.0 simulation software. The influence process and distribution law of mining stress and thick hard roof fracture on the elastic energy change in coal under a deep high-stress environment were studied, and the dynamic distribution state of high-energy elastic performance accumulation in a thick hard roof under the condition of gas containing coal instability and failure was obtained.

The rock deformation and fracture caused by coal mining may lead to the formation of stress concentration areas and high-stress areas in specific areas, which may lead to rock instability and other problems. Through simulation research, we can understand the stress changes in coal seams and overlying strata during the mining process of deep thick and hard roof working faces, which is of great significance for evaluating the possible stress concentration areas, high-stress areas, and stress transmission mechanisms in coal mining. At the same time, the study analyzed the change process and distribution law of a thick and hard roof on the elastic energy of coal, which helps to understand the impact of a thick and hard roof on the safety of coal seam mining and provides a basis for designing reasonable support methods and mining processes.

The underground mining activities in coal mines result in the accumulation of a large amount of elastic strain energy in coal layers, especially when the top plate is a hard and thick rock layer, which can easily cause dynamic disasters. Therefore, the safe mining of coal seams under a thick and hard roof is of great significance, but there is currently little research on the spatiotemporal evolution law of multiple fields, and a systematic analysis of the dynamic evolution law of the stress field, displacement field, energy field, and plastic zone during the mining process of deep thick and hard roof working faces. In addition, although the numerical simulation research results are not as accurate as the on-site measurement results, their general trend is the same. Compared to the on-site measurement, the numerical simulation requires less manpower, energy, and financial investment. The results can be mutually verified with the on-site measurement results, providing scientific basis for safety management and coal mining technology in coal mine production.

In this study, the working face is a nearly horizontal coal seam. Due to the simplification of the model, the dip angle of the coal seam in the model is taken as 0°. But even in nearly horizontal coal seams, there may still be some slight tilting or non-uniformity in actual situations. These small inclinations or non-uniformities may have a certain impact on stress distribution, roof stability, and gas extraction. In terms of direction, the mesh division of the model is not dense, and the height of the model is also simplified to a certain extent, which has a certain impact on the analysis of the plastic zone.

5. Conclusions

Thick and hard roofs are widely distributed in more than half of China's mining areas. When the roof is a hard and thick rock layer, it is easy to accumulate a large amount of elastic energy during coal seam mining, leading to dynamic disasters such as rock burst. This study utilized FLAC3D V4.0 numerical simulation software to simulate the dynamic evolution process of the stress field, displacement field, energy field, and plastic zone in coal seams and overlying strata during the mining process of deep thick and hard roof working faces, and analyzed the influence process and distribution law of mining stress and a thick hard impact roof on the change in coal elastic energy under a deep high-stress environment. The corresponding conclusions are as follows:

(1) With the continuous mining of the working face, the support pressure in front of the working face continues to increase, the stress in the overlying strata behind the working face continues to decrease, and the range of overlying strata failure continues to expand; the farther away from the coal seam, the smaller the impact of overlying strata stress due to mining disturbance.
(2) With the continuous mining of the working face, the rock mass on the top and bottom of the coal seam shows obvious displacement characteristics: the overlying strata mass inside the working face roof mainly shows downward vertical displacement, and the rock mass inside the bottom plate produces floor heave, mainly showing upward vertical displacement.
(3) With the continuous mining of the working face, there is a clear energy concentration area around the working face roadway. When the working face is mined to 60 m, the energy at both ends of the roadway intersects with the roof, forming an inverted "U" shape. The area expands as the mining distance of the working face increases, reaching its maximum at 100 m. At this point, collapse occurs and the energy density decreases slightly.
(4) With the continuous mining of the working face, the damage range of the plastic zone of the rock layer gradually expands. When the working face is mined to 60 m, the plastic zone presents a "saddle shaped" distribution, mainly characterized by shear failure. After mining to 80 m, the rock layer above the goaf shows significant

subsidence, and the surrounding rock stress is redistributed. The plastic zone is divided into penetrating the top, and the tensile failure gradually increases.

Author Contributions: Conceptualization, Z.Z. and H.S.; methodology, Z.Z., L.D., H.S., Y.L., H.Y. and R.L.; validation, Z.Z., L.D., H.S., Y.L., H.Y., R.L. and Y.Z.; formal analysis, L.D. and H.Y.; investigation, L.D., Y.L., H.Y., R.L. and Y.Z.; resources, Z.Z. and H.S.; data curation, L.D., Y.L. and R.L.; writing—original draft preparation, Z.Z., L.D., H.S., Y.L., H.Y., R.L. and Y.Z.; writing—review and editing, Z.Z., L.D., H.S., Y.L., H.Y., R.L. and Y.Z.; visualization, L.D., H.S., Y.L. and H.Y.; supervision, Z.Z. and H.S.; project administration, Z.Z., L.D. and H.S.; funding acquisition, Z.Z., H.S. and L.D. All authors have read and agreed to the published version of the manuscript.

Funding: This research was funded by Natural Science Foundation of Chongqing (No. CSTB2022NSCQ-MSX1080, No. cstc2021jcyj-msxmX1149, No. cstc2021jcyj-msxmX0564), Key Project of Science and Technology Innovation and Entrepreneurship Fund of Tiandi Technology Co., Ltd. (No. 2023-2-TD-ZD001), National Natural Science Foundation of China (No. 52274246), Open Research Fund of State Key Laboratory of Gas Disaster Detecting, Preventing and Emergency Controlling (No. 2022SKLKF11), and Chongqing Science Fund for Distinguished Young Scholars (No. cstc2019jcyjjqX0019).

Institutional Review Board Statement: The study did not require ethical approval.

Informed Consent Statement: Informed consent was obtained from all subjects involved in the study.

Data Availability Statement: All data and/or models used in the study appear in the submitted article.

Conflicts of Interest: The authors declare no conflict of interest.

References

1. Wei, J.B.; Wang, S.M.; Song, S.J.; Sun, Q.; Yang, T. Experiment and numerical simulation of over-burden and surface damage law in shallow coal seam mining under the gully. *Bull. Eng. Geol. Environ.* **2022**, *81*, 207. [CrossRef]
2. Xie, H.P.; Gao, F.; Ju, Y. Research and development of rock mechanics in deep ground engineering. *Chin. J. Rock Mech. Eng.* **2015**, *34*, 2161–2178.
3. Wang, F.; Jie, Z.Q.; Ma, B.; Zhu, W.H.; Chen, T. Influence of Upper Seam Extraction on Abutment Pressure Distribution during Lower Seam Extraction in Deep Mining. *Adv. Civ. Eng.* **2021**, *2021*, 8331293. [CrossRef]
4. Tang, Y.S.; Sun, W.C.; Zhang, X.; Liu, P.J. Effect of Advancing Direction of Working Face on Mining Stress Distribution in Deep Coal Mine. *Adv. Civ. Eng.* **2021**, *2021*, 7402164.
5. Li, C.Y.; Cui, C.Y.; Lei, G.R.; Zuo, J.P.; He, T.; Li, X.S.; Du, W.S. Tensile fracture mechanism of rock mass induced by the unloading-seeping of confining pressure in deep coal mining. *J. China Coal Soc.* **2022**, *47*, 3069–3082.
6. Dai, L.C.; Zhang, Z.G.; Sun, H.T.; Gao, H.L. Research on Mechanical Properties and Energy Evolution Law of Coal-Rock Assemblage with Different Gas Pressures. *Sustainability* **2022**, *14*, 9904. [CrossRef]
7. Du, F.; Wang, K.; Guo, Y.Y.; Wang, G.D.; Wang, L.; Wang, Y.H. The mechanism of rockburst-outburst coupling disaster considering the coal-rock combination: An experiment study. *Geomech. Eng.* **2020**, *22*, 255–264.
8. Li, J.W.; Fu, B.J.; Zhang, H.L.; Zhao, Q.C.; Bu, Q.W. Study on Fracture Behavior of Directly Covered Thick Hard Roof Based on Bearing Capacity of Supports. *Appl. Sci.* **2023**, *13*, 2546. [CrossRef]
9. Zhang, H.W.; Zhao, S.F.; Guan, L.G.; Chen, Z.; Gao, M.S.; Wang, X.Y.; Zhang, H.F. Characteristics of strong mining pressure in 6.0 m high mining height and thick hard roof working face. *J. Min. Strat. Control Eng.* **2022**, *4*, 37–46.
10. Zhang, G.F.; Liu, J.T.; Chang, A.P.; Zhang, W.L. Study on Key Parameters of Gob-Side Entry Retaining by Cutting Thick and Hard Roof in Inclined Coal Seam of Dongbaowei Coal Mine. *Min. Res. Dev.* **2021**, *41*, 111–116.
11. He, Z.L.; Lu, C.P.; Zhang, X.F.; Guo, Y.; Meng, Z.H.; Xia, L. Numerical and Field Investigations of Rockburst Mechanisms Triggered by Thick-Hard Roof Fracturing. *Rock Mech. Rock Eng.* **2022**, *55*, 6863–6886. [CrossRef]
12. Guo, Y.; Lu, C.P.; He, Z.L.; Song, J.F. Numerical and Field Investigations of Tremors Induced by Thick-Hard Strata Fracture. *Appl. Sci.* **2022**, *12*, 11151. [CrossRef]
13. Gao, R.; Yang, J.X.; Kuang, T.J.; Liu, H.J. Investigation on the Ground Pressure Induced by Hard Roof Fracturing at Different Layers during Extra Thick Coal Seam Mining. *Geofluids* **2020**, *2020*, 8834235. [CrossRef]
14. Ma, B.P.; Zhang, J.B.; Liu, Y.H.; Liu, S.W.; Liao, W.L.; Li, J. Deformation mechanism and control of surrounding rock in soft gently inclined coal seam roadway with thick hard roof. *Coal Eng.* **2022**, *54*, 109–116.
15. Wang, R.; Liu, Q.J.; Cheng, L.; Ding, W.B.; Feng, Y.T.; Zhang, Z.; Liu, X.G. Strong mine pressure behavior law and control technology of longwall top-coal caving face in shallow extra-thick coal seam with thick hard roof. *Coal Eng.* **2023**, *55*, 47–52.

16. Tan, Y.L.; Zhang, M.; Xu, Q.; Guo, W.Y.; Yu, F.H.; Gu, S.T. Study on occurrence mechanism and monitoring and early warning of rock burst caused by hard roof. *Coal Sci. Technol.* **2019**, *47*, 166–172.
17. Zhang, C.N.; Cao, A.Y.; Li, W.D.; Li, Z.L.; Ma, Y.Z.; Wang, Q.; Li, Y.Y. Study on Stress Distribution Law and Its Influencing Factors in Mining of Coal Seam with Large Cover Depth, Thick Topsoil and Hard-Thick Roof Conditions. *Coal Technol.* **2023**, *42*, 86–91.
18. Kang, Z.P.; Zhao, J.; Duan, C.R. Overburden structure failure and movement law of thick and hard roof in slicing mining. *Coal Eng.* **2022**, *54*, 78–83.
19. Liang, S.P.; Lu, Y.L.; Guo, P.; Wu, B.Z. Mechanical Analysis of the First Fracture Characteristics of Hard Roof of Extra-thick Coal Seam. *Saf. Coal Mines* **2020**, *51*, 245–250.
20. Li, A.; Ma, Q.; Lian, Y.Q.; Ma, L.; Mu, Q.; Chen, J.B. Numerical simulation and experimental study on floor failure mechanism of typical working face in thick coal seam in Chenghe mining area of Weibei, China. *Environ. Earth Sci.* **2020**, *79*, 118. [CrossRef]
21. Xiong, Y.; Kong, D.Z.; Wen, Z.J.; Wu, G.Y.; Liu, Q.Z. Analysis of coal face stability of lower coal seam under repeated mining in close coal seams group. *Sci. Rep.* **2022**, *12*, 509. [CrossRef] [PubMed]
22. Yang, K.; Liu, W.J.; Jiao, B.; Zhang, Q.H.; Liu, S.; Zhang, Z.N. Three-dimensional physical simulation of overburden migration in deep thick hard roof fully-mechanized caving mining. *Chin. J. Geotech. Eng.* **2021**, *43*, 85–93.
23. Bu, Q.W.; Tu, M.; Zhang, X.Y.; Yuan, B.Q.; Zhao, Q.C.; Dang, J.X. Study on fracture instability and energy accumulation-release evolution of thick-hard roof in stope. *J. Min. Saf. Eng.* **2022**, *39*, 867–878.
24. Li, T.; Li, Z.; Sun, J.D. Study on Dynamic Evolution of Overburden Rock Movement and Mining-Induced Stress of Ultra-high Working Face. *Shock. Vib.* **2022**, *2022*, 2271635. [CrossRef]
25. Xie, J.L.; Ning, S.; Zhu, W.B.; Wang, X.Z.; Hou, T. Influence of Key Strata on the Evolution Law of Mining-Induced Stress in the Working Face under Deep and Large-Scale. Mining. *Minerals* **2023**, *13*, 983. [CrossRef]
26. Li, W.T.; Li, X.M.; Mei, Y.C.; Wang, G.; Yang, W.D.; Wang, H.T. A numerical simulation approach of energy-absorbing anchor bolts for rock engineering. *Int. J. Rock Mech. Min. Sci.* **2022**, *158*, 105188. [CrossRef]
27. Yang, Z.Q.; Liu, C.; Zhu, H.Z.; Xie, F.X.; Dou, L.M.; Chen, J.H. Mechanism of rock burst caused by fracture of key strata during irregular working face mining and its prevention methods. *Int. J. Min. Sci. Technol.* **2019**, *29*, 889–897. [CrossRef]
28. Shao, X.N. *Research of Fracture Law and Deep Hole Advance Blasting Technology in Hard Thick Sandstone Roof*; AnHui University of Science and Technology: Huainan, China, 2014.
29. Wu, Q.H. *Analyzing Stability Synthetically and Researching Treatment Methods on the Complicated Multi-Layer Mine-Out Areas*; Central South University: Changsha, China, 2010.
30. Ye, Q.; Wang, W.J.; Wang, G.; Jia, Z.Z. Numerical simulation on tendency mining fracture evolution characteristics of overlying strata and coal seams above working face with large inclination angle and mining depth. *Arab. J. Geosci.* **2017**, *10*, 82. [CrossRef]
31. Wen, X.L.; Ge, Z.C.; Zhang, F.Y. Study on the Migration Law of Overlying Rock in the Upward Layered Continuous Mining Face of Thick Coal Seam with Paste Backfill Mining. *Math. Probl. Eng.* **2022**, *2022*, 7297477. [CrossRef]
32. Shi, B.W.; Bai, J.P.; Hao, C.S.; Yang, C.Y.; Yao, J.B. Three-dimensional Simulation of Dynamic Evolution of Mining-induced Overburden Fractures. *Saf. Coal Mines* **2019**, *50*, 259–262.